

Effects of Different Deinking Processes on Fiber Morphology, Hydrogen Bond Models, and Cellulose Supramolecular Structure

Qinglin Meng,^{a,b} Jinquan Wan,^{b,c,*} Yongwen Ma,^{b,c} and Yan Wang^{b,c}

Deinked pulp fibers produced by three kinds of deinking processes, alkaline deinking, neutral deinking, and enzymatic deinking, were studied by Scanning Electron Microscope (SEM), Fourier Transform Infrared Spectrometer (FTIR), X-ray Diffraction (XRD), and Cross-Polarization Magic Angle Spinning Carbon-13 Nuclear Magnetic Resonance (CP/MAS ¹³C-NMR). There were remarkable differences in both macroscopic and microscopic structure between the samples. SEM images showed that the effects of deinking processes on fiber morphology were obvious and the influences of alkaline deinking were the most apparent. FTIR analysis indicated that the content of intermolecular hydrogen bonds increased by 22.63%, 9.42%, and 14.40% after the alkaline deinking process, neutral deinking process, and enzymatic deinking process, respectively. XRD revealed that the average width of crystallite size in the (002) lattice plane was decreased after different deinking processes, in accordance with the change tendency of cellulose crystallinity. CP/MAS ¹³C NMR combined with spectral fitting demonstrated that the content of different cellulose polymorphs changed during deinking processes. The increase of WRV was attributed to changes in the hydrogen bonding patterns and cellulose supramolecular structure.

Keywords: Deinking; Fiber morphology; Hydrogen bond; Supramolecular structure; WRV

Contact information: a: School of Light Chemical and Food Science Engineering, South China University of Technology, Guangzhou 510640, PR China; b: State Key Laboratory of Pulping and Papermaking Engineering, South China University of Technology, Guangzhou 510640, PR China; c: School of Environmental Science and Engineering, South China University of Technology, Guangzhou 510006, PR China; *Corresponding author:mwizard@126.com

INTRODUCTION

With the demand of protecting forest resources and developing a low-carbon economy, secondary fiber recycling has aroused the attention of technologists throughout the world, and the rapid growth of the waste paper utilization has become an important trend of the world's paper industry. According to the statistics of the China Paper Association, the total consumption of pulp from wastepaper in the paper industry was 44.39 million tons in 2008 in China. In 2011 it increased to 56.60 million tons, accounting for 62% of total pulp consumption (China Paper Association). Recycled cellulose fiber accounted for about 70% of the papermaking materials by the end of the 20th century (Wan and Ma 2004). This recycled material can help make up for an insufficient supply of fresh papermaking raw materials, can reduce energy consumption in comparison to the pulping of wood, and also can play an essential role in decreasing environmental pollution problems. Deinking is an important stage in secondary fiber

recycling. Conventional deinking processes often employ sodium hydroxide in combination with a large amount of other chemicals, including sodium silicate, hydrogen peroxide, and surfactants (Shrinath *et al.* 1991). This high pH and chemical-intensive process leads to several major problems for the process and recycled paper quality, including a high degree of fragmentation of large sticky contaminants, darkening of pulp fiber, increased chemical oxygen demand (COD) in waste waters, and the need for substantial amounts of acid for neutralization (Lapierre *et al.* 2002). These disadvantages have hindered the further development of alkaline deinking processes. In this context, a new development of deinking under neutral or weakly acidic conditions (without sodium hydroxide, sodium silicate, and hydrogen peroxide, *etc.*) has shown promise for alleviating the negative impact of alkaline deinking (Dorris *et al.* 2003; Lapierre *et al.* 2006).

With recent advances in biotechnology, enzymes already have become widely used in deinking processes. Compared to the chemical-based deinking methods, enzymatic deinking could reduce the demand for chemicals, enhance ink and stickies removal, and also lower the process costs and environmental impacts (Bajpai and Bajpai 1998; Jeffries *et al.* 1994). Therefore, enzymatic deinking has been suggested as an environmentally friendly alternative to complement conventional chemical deinking in the recycling of recovered paper. Over the last couple of years, a large number of enzymes, including cellulase, hemicellulases, xylanase, pectinases, amylases, esterases, laccase, and lipase have been evaluated for their potential to replace hazardous chemicals in deinking recycled paper, and some achievements have been made.

During the deinking process, physical and chemical factors significantly influence the fiber structure. At present, most research on the subject has mainly focused on deinking efficiency and the changes of fiber properties, which usually have been indicated by the brightness and strength properties of the paper sheets (Mansfield *et al.* 1997; Ibarra *et al.* 2012). However, this change of plant fiber is mainly due to the irreversible structural changes in the fiber wall caused by the deinking method. Different deinking processes with various chemicals may influence the fiber ultrastructure differently. Hence, those studies could not expose the underlying reasons for the changes of paper-making properties, particularly the aspects of fiber structure in a fine level. By contrast, in our research, both the macroscopic and microcosmic structural changes were studied together, including fiber morphology, models to describe the patterns of hydrogen bonding, and cellulose supramolecular structure.

In recent years modern analysis methods have been widely used in pulp and paper areas of application. Scanning electron microscopy (SEM) is one of most popular surface analytical techniques. In the paper industry SEM is mainly used to study or characterize fibers and fillers, including their z-direction distribution in paper structure, by virtue of offering high quality images with high resolution (Chinga 2002; Eriksen *et al.* 2006; Bennis *et al.* 2010). So far, several approaches have been improved to carry out the SEM images. As reported, Claramunt *et al.* (2010) used SEM to investigate morphological changes after drying and rewetting cycles. The effect of laccase treatment on fiber surface was studied by SEM method (Wei *et al.* 2007). Beyond that, FTIR spectrometry, as a traditional analysis method in wood research, has been used for characterizing the cellulose structural features (Mohkami and Talaeipour 2011; Liu *et al.* 2005). In addition, FTIR absorption provides useful information related to the change of hydrogen bonding (Maréchal and Chanzy 2000). By using software in combination with a Gaussian

distribution function, the FTIR spectra region of 3800 to 3000 cm^{-1} was resolved into three or four bands to distinguish the relative contributions of different hydrogen bonds (Maréchal and Chanzy 2000; Oh *et al.* 2005; Popescu *et al.* 2009). Furthermore, XRD and CP/MAS ^{13}C NMR were used to determine the supramolecular structure of cellulose, including the crystallinity, crystal size, and the content of polymorphs (Wan *et al.* 2010; Miyamoto *et al.* 2011; Hult *et al.* 2002). For example, Newman used solid-state carbon-13 NMR spectroscopy to characterize a bleached softwood kraft pulp in the never-dried state and after cycles of drying and remoistening (2004). Moreover, Rebuzzi and Evtuguin (2006) used XRD and solid-state carbon-13 NMR to determine the cellulose crystallinity of *Eucalyptus globulus* bleached pulps.

In this work, we used a combination of different analytical techniques, *i.e.* Scanning Electron Microscope (SEM), Fourier Transform Infrared Spectroscopy (FTIR), X-ray Diffraction (XRD), and Cross-Polarization Magic Angle Spinning Carbon-13 Nuclear Magnetic Resonance (CP/MAS ^{13}C NMR) to investigate the changes of fiber morphology, hydrogen bond models, and cellulose supermolecular structure of eucalyptus kraft pulps treated with three kinds of deinking processes. It was possible, based on this work, to clarify the relationships among WRV, hydrogen bonds models, and cellulose supramolecular structure.

EXPERIMENTAL

Materials

Eucalyptus wood chips were cooked in autoclaves according to the conventional kraft process under the following conditions: 17% NaOH and 5% Na_2S , wood-to-liquor ratio of 1:4, temperature ramp-up time of 2 h, cooking temperature of 170 °C, and time at cooking temperature of 2 h. The pulp was used for deinking treatments, though no ink was used in the study.

Preparation of the neutral deinking agent was carried out as follows: sequentially adding Sodium Alcohol Ether Sulphate (AES), Coconutt Diethanol Amide (6501), and Fatty Alcohol Polyoxy-ethylene Ether (AEO-9) into a three-necked flask (the mass ratios were 2:1:1), mixing when adding materials, in which time intervals for adding the material were more than 10 min. The contents were fully mixed material in a mechanical device at 65 °C for 50 min for synthesis of the neutral deinking agent.

The cellulase was mainly supplied by Leveking Bio-Engineering Co. Ltd., and the serial number is LPK-CD06.

Methods

Pulp treatment (Deinking processes)

Three kinds of deinking processes – an alkaline deinking process, a neutral deinking process, and an enzymatic deinking process – were used for deinking in this study. The recipes for different deinking methods were as follows: (1) alkaline deinking process using 2% NaOH, 3% dry $\text{Na}_2\text{Si}_2\text{O}_3$, 0.5% neutral deinking agent, and 2.0% H_2O_2 for 60 min at 40 °C and 10% consistency (all based on o.d. paper, the same below), (2) neutral deinking process using 1.0% neutral deinking agent for 40 min at 50 °C and 10% consistency, (3) enzymatic deinking process using 1.0% cellulase, then adding NaOH to pH 8 for 30 min at 45 °C and 12% consistency.

Deinking chemicals, 10 g o.d. pulp, and hot water were added into the sealing bag to achieve the required slurry consistency and reaction temperature. Then the sealing bags were put into an electric-heated thermostatic water bath. After reaction, flotation was carried out in ZQS-10 Flotation Cell. The flotation conditions were 0.2% CaCl₂ on pulp, 1% consistency, and certain air pressure and air flow. The time allowed for flotation was 15 min, 20 min, and 40 min, respectively (Wei 2009). Finally, all the pulp samples were exhaustively washed with distilled water through a 200-mesh wire screen. The pulp samples were then transferred into plastic bags for storage.

Morphology

The samples were coated with gold film in order to observe the surface morphology and the microstructure. The instrument was a LEO 1530 VP Scanning Electron Microscope (SEM).

Fourier transform infrared spectrophotometer (FTIR)

Freeze-dried pulp samples (3.5 to 4.0 mg) and KBr (350 mg) were homogenized using an agate mortar and thereafter pressed into a transparent tablet at 200 kgf/cm² for 5 min. Spectra were recorded using a Bruker Vector 33 Fourier Transform Infrared Spectrophotometer (FTIR) set at a resolution of 4 cm⁻¹ over the range 4000 to 400 cm⁻¹.

The crystallinity index was calculated from the relative intensities of the infrared bands, finding the ratios of 1372/2900 cm⁻¹,

$$\text{N.O'KI} = \frac{I_{1372}}{I_{2900}} \times 100\% \quad (1)$$

where I_{1372} represents the intensity (1372 cm⁻¹) of the band belonging to the CH bending vibration and I_{2900} is the intensity (2900 cm⁻¹) of the band belonging to the CH and CH₂ bending vibrations.

Determination of cellulose crystallinity by X-ray diffraction (XRD)

The X-ray diffraction (XRD) scattering pattern of the pulp was obtained using a Philipps X'Pert MPD diffractometer with a Cu-K α source ($\lambda = 0.154$ nm) in the 2θ range of 4 to 60° and a scanning step width of 0.02°/scan. The crystalline reflections and amorphous halo of samples were defined according to previously described recommendations (Wan *et al.* 2010 and Liao *et al.* 2011). The cellulose crystallinity (%) was calculated by means of the following equation (Kim and Hotzapple 2006),

$$\text{CI(XD)} = \frac{I_{002} - I_{am}}{I_{am}} \times 100\% \quad (2)$$

where I_{002} and I_{am} are the maximum scattering intensities of the diffraction from the (002) plane at $2\theta = 22.6^\circ$ and the diffraction intensity of the background scatter measured at $2\theta = 18^\circ$, respectively.

The average width of crystallites obtained from (hkl) diffraction was determined from the following formula (Bhuiyan and Hirai 2005),

$$L_{hkl} = \frac{K\lambda}{\beta_{\theta} \cos \theta} \quad (3)$$

where K is the Scherrer constant (0.9), λ is the wave length of the X-ray source (0.154 nm), β is the full-width at half-maximum of the reflection hkl measured, and 2θ is the corresponding Bragg angle.

Determination for CP/MAS ^{13}C NMR

During sample preparation the pulps for CP/MAS ^{13}C -NMR analysis were subjected to a mild chlorite delignification with NaClO_2 (1.5 g/g sample) under acidic conditions at room temperature followed by treatment with 0.1 M NaOH overnight. Between the NaClO_2 and NaOH stages, the samples were rinsed with deionized water to pH 4 to 5. The overall procedure was repeated twice. Afterwards, the samples were hydrolyzed for 8 h in 2.5 M HCl at 100 °C (Hult *et al.* 2001). Finally, the pulp samples were washed with deionized water to a pH of 4 to 5 prior to drying freely.

All spectra of samples (water content 40 to 60% by weight) were recorded on a Bruker AVANCE AV 400 instrument (at ambient temperature) operating at 9.4 T for ^{13}C -NMR. The pulp samples were packed in a zirconium oxide rotor. The MAS rate was 6 kHz. Acquisition was performed with a CP pulse sequence using a 3.3 ms proton 90° pulse, 1500 ms contact pulse, and a 2.0 s delay between repetitions. Glycine was used for the Hartman–Hahn matching procedure and as external standard for the calibration of the chemical shift scale relative to tetramethylsilane $(\text{CH}_3)_4\text{Si}$.

Determination of WRV

The water retention value (WRV) is an important property closely associated with cellulose crystallinity and swelling capability (Forsström *et al.* 2005; Gumuskaya *et al.* 2003). The WRV value was determined by the centrifugal method (Wistara and Yong 1999) on pulp or paper with a dry weight equivalent of 1.5 g. Centrifugation was stopped after 15 min at 3000 rpm. After centrifugation, the fiber mat was weighed in a pre-weighed weighing bottle and dried in an oven at 105 ± 2 °C for 24 h and then re-weighed. WRV was calculated with the following equation,

$$\text{WRV} = \frac{m_1 - m_2}{m_2} \times 100\% \quad (4)$$

where m_1 is the weight of wet pulp after centrifugation and m_2 is the weight of the dry pulp (in grams).

RESULTS AND DISCUSSION

Morphological Characterization

Scanning Electron Microscopy (SEM) is widely used to observe the surface characteristics of fibers after different physical and chemical treatments. In the present study, SEM images of the native and deinked pulp fibers were taken to investigate the morphological changes during different deinking processes. Figure 1 presents the surfaces of eucalyptus pulp fibers treated with three different deinking methods. As

shown in Fig. 1A, the fibers of eucalyptus native pulp were thick, the fiber surface was smooth and regular, and the fiber structure was dense. Compared with the fibers of native pulp, the fibers of deinked pulp were damaged differently. After the alkaline deinking process, the fibers appeared to have been damaged, as viewed from the surface (Fig. 1B). The fibers became much thinner, the fiber surface was slightly fibrillated, fines appeared between fibers, and the fiber structure was loosened. The fibers of neutral deinked pulp are shown in Fig. 1C. Compared with the fibers of alkaline deinked pulp, the fibers of neutral deinked pulp were damaged slightly, and the amount of fines was also less than in the case of the alkaline deinked pulp. The fiber surface and structure were similar to the fibers of native pulp. After enzyme treatment, there were more pores on the fibers surface and the interspaces among the fibers increased (Fig. 1D). Those phenomena are mainly attributed to the cellulose hydrolysis on the surface of the fibers, a procedure known as “peeling-off fibers”, which facilitates ink detachment from the surface and leads to a removal of small fibrils.

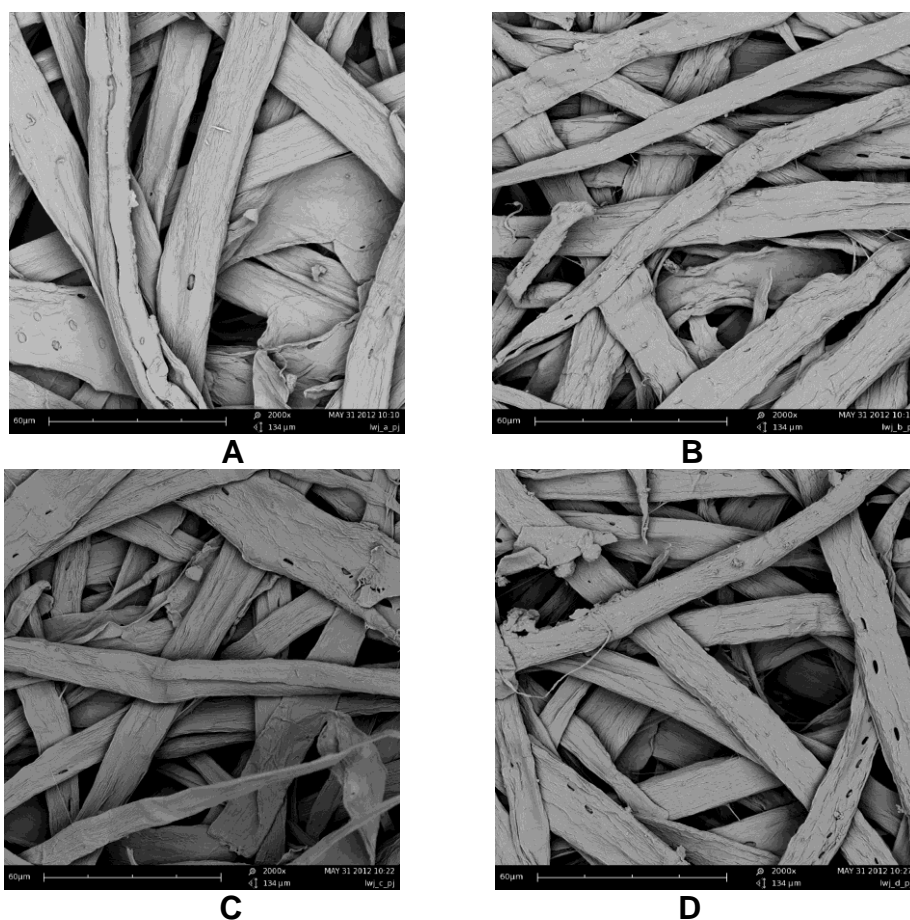


Fig. 1. Scanning electron micrographs of the fibers of (A) native pulp, (B) alkaline deinked pulp, (C) neutral deinked pulp, and (D) enzymatic deinked pulp

Content of Different Hydrogen Bond Models of Deinked Pulp Fibers

In the FTIR spectra, as shown in Fig. 2, a broad band could be observed at around 3400 cm^{-1} , which was attributed to the stretching vibrations of the hydroxyl (O–H) groups, and the maximum absorbance of hydrogen-bonded O–H stretching was shifted to a higher wavenumber after the deinking processes, as presented in Table 1. According to

previous research, this band would be significantly influenced by the transformation related to the change of intra- and intermolecular hydrogen bonds: the band shifts to a lower wave number when the intensity of the intermolecular hydrogen bonds increases. Thus, the result in this experiment indicated that the intermolecular hydrogen bonds were destroyed during the deinking processes. Moreover, the crystallinity index obtained by FTIR spectroscopy (N.O'KI) decreased, as shown in Table 1, in an order of alkaline deinking > enzymatic deinking > neutral deinking. These results are consistent with a hypothesis that there were differences in the manner or degree to which the cellulose crystalline regions were partly destroyed when subjected to different deinking process (Guo *et al.* 2011).

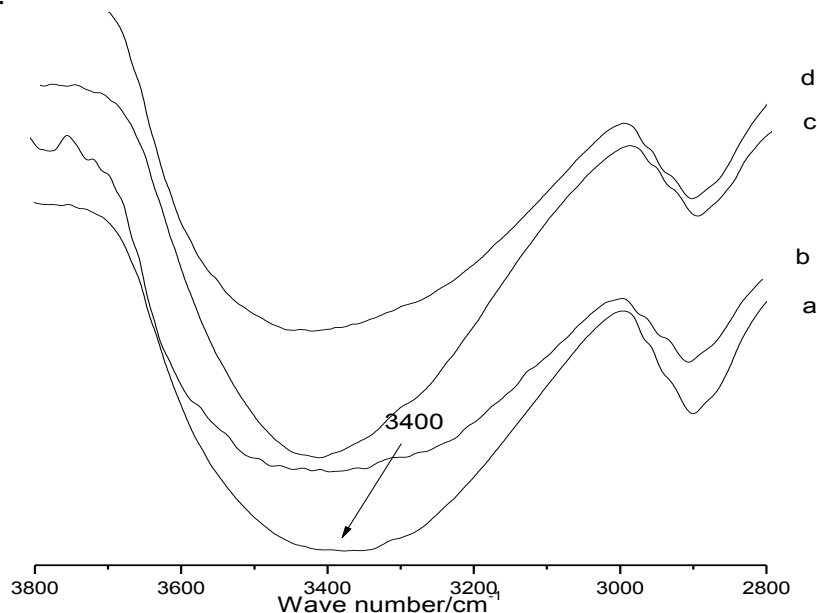


Fig. 2. FTIR spectra of all the pulp samples: (a) native pulp, (b) alkaline deinked pulp, (c) neutral deinked pulp, and (d) enzymatic deinked pulp; spectra regions: 3800-2800 cm^{-1}

Table 1. Effect of Deinking Processes on the Displacement of Hydrogen Bond Absorption Peak in IR Spectra and the Crystallinity Index (N.O'KI)

Deinking method	Without deinking	Alkaline deinking	Neutral deinking	Enzymatic deinking
Hydrogen bond peak position(cm^{-1})	3387	3439	3415	3423
N.O'KI	1.134	0.951	1.078	1.032

Though the shift of hydrogen-bonded O–H stretching vibrations was observed in the FTIR spectra, the accurate contents of different hydrogen bonds were still unknown. Recently, in order to analyze the content of hydrogen bonds conforming to different models of cellulose crystallinity, more and more effort has been devoted to separating the overlapping bands derived from hydrogen bonds in FTIR spectra (Kondo and Sawatari 1996; Schwanninger *et al.* 2004). According to previous research, the intramolecular hydrogen bonds for 2-OH \cdots O-6 and 3-OH \cdots O-5, and the intermolecular hydrogen bonds for 6-OH \cdots O-3' in cellulose I appear at 3455–3410, 3375–3340, and 3310–3230 cm^{-1} , respectively, along with the valence vibration of H-bonded OH groups at 3570–3450

cm^{-1} . Compared with the bands of cellulose I, a new band related to intermolecular hydrogen bonding of $2\text{-OH}\cdots\text{O-2}'$ and/or intermolecular hydrogen bonding of $6\text{-OH}\cdots\text{O-2}'$ in cellulose II appears at around 3115cm^{-1} after NaOH treatment (Oh *et al.* 2005).

In this study, the FTIR spectra were resolved by using the PeakFit software's Gaussian function (Maréchal and Chanzy 2000; Popescu *et al.* 2009) to differentiate the hydrogen bond types. Assuming that all the vibration modes follow a Gaussian distribution, mixed modes of hydrogen bonded O–H stretching were resolved into three bands for cellulose I and four bands for cellulose II. The FTIR spectra of the hydrogen-bonded O–H stretching vibrations with the corrected baseline are shown in Fig. 3. Table 1 quantifies the results of the FTIR spectra for the amounts of hydrogen bond O–H stretching vibrations (with the baseline correction).

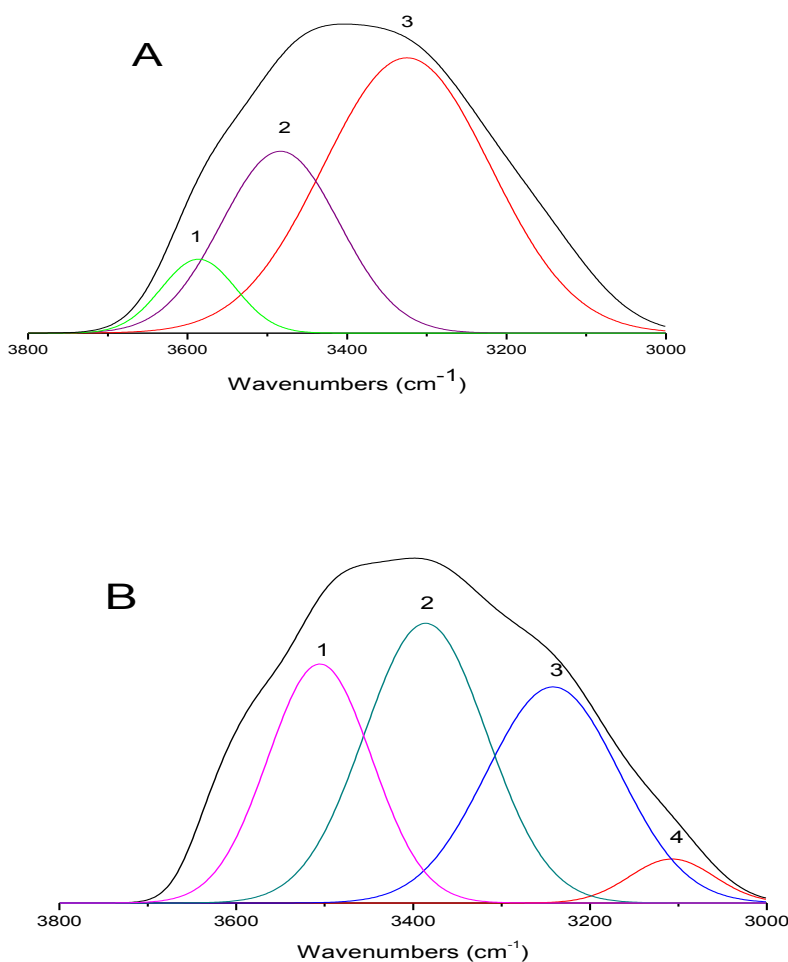


Fig. 3 (A & B). Resolution of hydrogen-bonded OH stretching of FTIR spectrum of fibers: (A) native fibers, (B) alkaline deinked pulp fibers (C) neutral deinked pulp fibers and (D) enzymatic deinked pulp fibers; bonding modes: (1) intramolecular hydrogen bond $2\text{-OH}\cdots\text{O-6}$; (2) intramolecular hydrogen bond $3\text{-OH}\cdots\text{O-5}$; and (3) intermolecular hydrogen bond $6\text{-OH}\cdots\text{O-3}'$; (4) intermolecular hydrogen bond of $2\text{-OH}\cdots\text{O-2}'$ and/or intermolecular hydrogen bond of $6\text{-OH}\cdots\text{O-2}'$

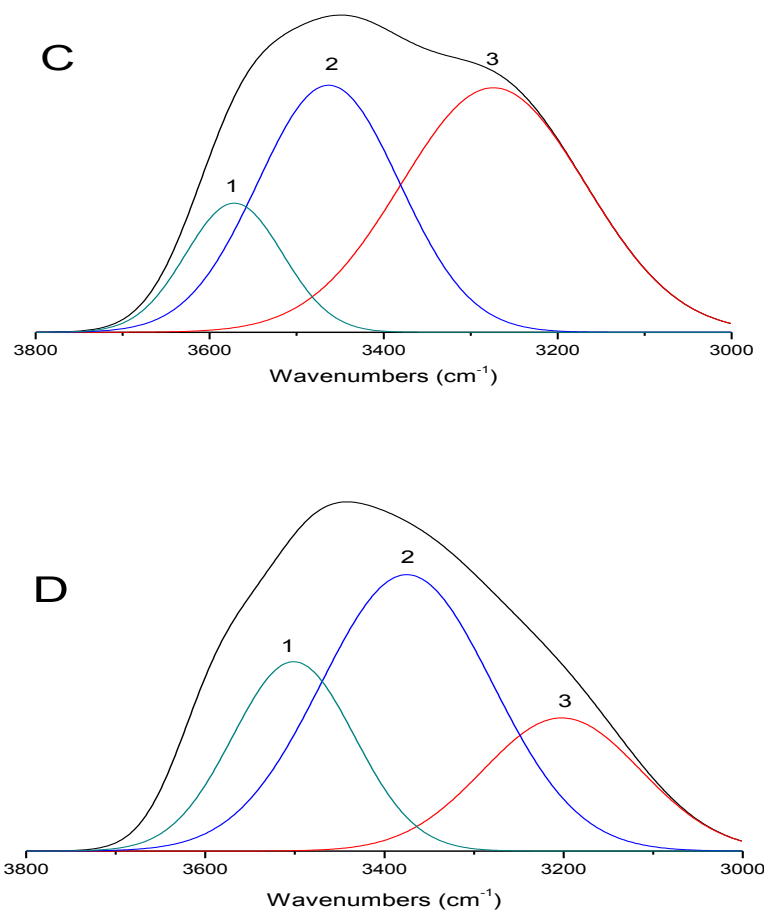


Fig. 3 (C & D). Resolution of hydrogen-bonded OH stretching of FTIR spectrum of fibers: (A) native fibers, (B) alkaline deinked pulp fibers (C) neutral deinked pulp fibers and (D) enzymatic deinked pulp fibers; bonding modes: (1) intramolecular hydrogen bond 2-OH···O-6; (2) intramolecular hydrogen bond 3-OH···O-5; and (3) intermolecular hydrogen bond 6-OH···O-3'; (4) intermolecular hydrogen bond of 2-OH···O-2' and/or intermolecular hydrogen bond of 6-OH···O-2'

From the resolution of hydrogen-bonded OH stretching, as shown in Fig. 3, the FTIR spectrum of alkaline deinked pulp fibers was resolved into four bands. This result indicated that a portion of cellulose I was transformed to cellulose II during alkaline deinking process due to the NaOH treatment. This phenomenon is similar to that shown in previous research (Oh *et al.* 2005). Despite the transformation of the cellulose crystal system, the content of different hydrogen bond models changed as well. The total content of the intramolecular hydrogen bonds increased approximately by 22.63%, 9.42%, and 14.40% after the alkaline deinking process, neutral deinking process, and enzymatic deinking process, respectively. At the same time, the content of intermolecular hydrogen bonds decreased by approximately 22.73%, 7.08%, and 12.12%. However, among the three kinds of deinking processes, the content of the intramolecular hydrogen bonds exhibited the largest increase during the alkaline deinking process, followed by enzymatic deinking and neutral deinking. This tendency is in accordance with the change

in regularity of cellulose crystallinity obtained by FTIR [CI(IR)]. These explanations are related to the cellulose crystalline regions being formed with cellulose polymer chains by connecting with the intramolecular hydrogen bonds. Therefore, the FTIR fitting result showed that the transformation of crystalline regions to amorphous regions took place within cellulose during deinking processes.

Table 2. Content of Different Hydrogen Bond Models Obtained by FTIR Gaussian Fitting

Deinking Method	Hydrogen Bond	Wave Number (cm ⁻¹)	Content (%)
Without deinking	2-OH···O-6	3487.2	20.56
	3-OH··O-5	3329.8	30.61
	6-OH···O-3'	3196.2	41.10
Alkaline deinking	2-OH···O-6	3495.5	24.21
	3-OH··O-5	3349.2	38.54
	6-OH···O-3'	3231.6	31.76
	2-OH···O-2' or 6-OH··O-2'	3108.9	3.72
Neutral deinking	2-OH···O-6	3496.4	19.11
	3-OH··O-5	3315.7	36.88
	6-OH···O-3'	3209.4	38.19
Enzymatic deinking	2-OH···O-6	3501.4	21.42
	3-OH··O-5	3375.0	37.12
	6-OH···O-3'	3204.7	36.12

Changes in Cellulose Supramolecular Structure during Deinking Processes

Figure 4 shows the X-ray diffractograms of all the pulp samples. Two main peaks were observed for all the curves at around $2\theta = 16^\circ$ and at $2\theta = 22.6^\circ$. The approximately 16° reflection corresponds to the overlapping of the (10 $\bar{1}$) and (110) crystallographic planes, and the peak at 22.6° corresponds to the (002) plane. Although the analysis of FTIR spectra indicated that cellulose II appeared after the alkaline treatment, all the X-ray diffraction curves exhibited typical cellulose I structure. This is explained by the fact that the transformation (cellulose I to cellulose II) was not complete following the NaOH treatment employed in this study. The high temperature and low concentration of NaOH treatment may retard the transformation (Freitag and Donzé 1983). Therefore, in this study, only the change of the crystallite size in cellulose I was considered.

As mentioned previously, changes in cellulose supramolecular structure were analyzed by X-ray Diffraction (XRD). The X-ray diffraction curve represents the sum of all crystal allomorphs in the cellulose sample. In order to establish the crystalline and the amorphous areas more precisely, the peaks of X-ray diffraction curve were resolved, as shown in Fig. 5 (these peaks were all separated by Gaussian resolution). After resolution, there were three main bands: the 14.6° (2θ) reflection assigned to the (101) crystallographic plane, the 16.5° (2θ) reflection assigned to the (10 $\bar{1}$) crystallographic plane, and the 22.6° (2θ) reflection assigned to the (002) or (200) crystallographic planes of cellulose I (Colom *et al.* 2003; Marcovich *et al.* 2001).

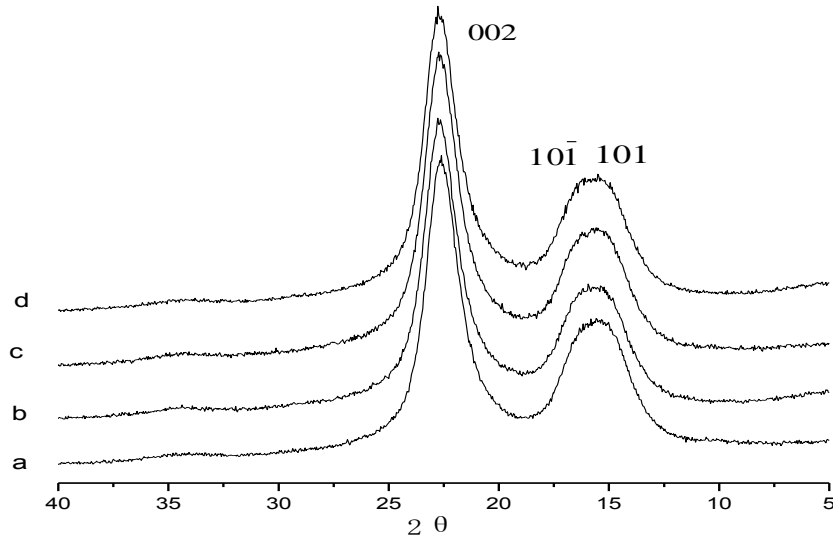


Fig. 4. X-ray diffractograms of fibers treated with different deinking processes: (a) without deinking (b) alkaline deinking (c) neutral deinking and (d) enzymatic deinking

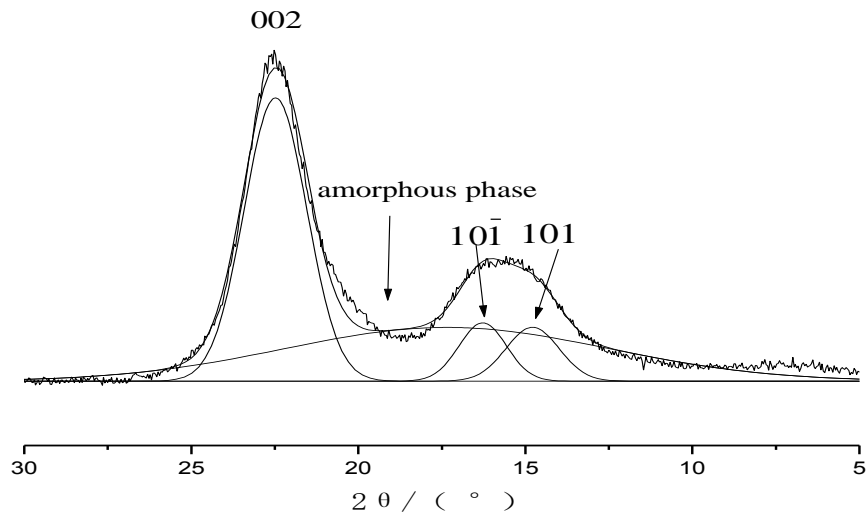


Fig. 5. Resolution of XRD diffractogram of pulp sample for cellulose I

The function that calculates mean cross sectional area (A) is given by,

$$A = L_{002} \times 1/2(L_{101\bar{1}} + L_{101}) \quad (5)$$

where (L_{002} , $L_{101\bar{1}}$) and L_{101} are the average width of crystal in (002), ($101\bar{1}$), and (101), respectively) (Hult *et al.* 2003). The crystallinity index [CI(XD)] was calculated from the ratio of the area of all crystalline peaks to the total area. The resolution results of X-ray diffraction curves and the crystallinity index [CI(XD)] are presented in Table 3.

Table 3. Analyses of Cellulose Supramolecular Structure in Eucalyptus Kraft Pulps with Different Deinking Processes

Deinking method	Lattice plane (nm)	Diffraction angle 2θ (°)	L_{hkl} (nm)	CI(XD) (%)	A (nm ²)
Without deinking	10 $\bar{1}$	14.643	14.1	68.3	54.57
	101	16.257	7.0		
	00 $\bar{2}$	22.642	5.1		
Alkaline deinking	10 $\bar{1}$	14.607	7.7	57.9	43.01
	101	16.688	6.4		
	00 $\bar{2}$	22.632	4.1		
neutral deinking	10 $\bar{1}$	14.445	10.3	64.2	49.59
	101	16.802	6.8		
	00 $\bar{2}$	22.670	4.8		
Enzymatic deinking	10 $\bar{1}$	14.585	10.5	61.6	45.05
	101	16.950	6.5		
	00 $\bar{2}$	22.739	4.6		

According to Table 3, the average width of crystallites with respect to the 00 $\bar{2}$, 101, and 10 $\bar{1}$ planes decreased appreciably after the deinking processes, and the influence of alkaline deinking was more significant than that of neutral deinking and enzymatic deinking. As a result, the mean cross-sectional area of the three pulp samples decreased, negatively influencing accessibility and homogeneity of the fibers. Moreover, the crystallinity index [CI(XD)] had the same tendency as the average width of crystallite and the mean cross sectional area. Similar results were found by Guo *et al.* in ONP deinked by three kinds of deinking methods (2010). This result is mainly attributable to the various effects of different kinds of deinking processes on the fibers, and it also indicated that the above deinking methods destroyed the cellulose crystalline regions. During the neutral deinking process, the surfactants were used only to disperse and prevent the reprecipitation of the ink, so the fibers showed little damage. On the contrary, NaOH and Na₂SiO₃ were added during the alkaline deinking process as well as surfactants. Those chemicals can act on the fibers directly to destroy the hydrogen bonds and the crystalline regions (Pan 2008), resulting in decreased cellulose crystallinity and the deformation of the fibers due to swelling. Because the fibrillation on the fibers and pores appeared at the cross section and were caused by the degradation of cellulose by using cellulase during enzymatic deinking process, the crystalline regions of the fibers were partly damaged. Evidence of such changes could be observed in the SEM micrographs.

Changes of the Content of Polymorphs and Cellulose Fibril Aggregation after Deinking Processes

In order to study the significant differences in effects of deinking processes on the ultrastructure of cellulose fibrils, solid-state cross polarization magic angle spinning carbon-13 nuclear magnetic resonance (CP/MAS ¹³C NMR) was used in combination with spectral fitting. In the spectra of ¹³C NMR, as shown in Fig. 6, the signals assigned to C4 were partly separated into two clusters, labeled i and s, which were assigned to the interiors and surfaces of the crystalline domains, respectively. With spectral fitting, those NMR spectra were analyzed in detail, and some structural parameters such as the allomorph composition, relative amounts of different cellulose allomorphs present, and lateral dimensions for cellulose elementary fibrils and microfibrils were determined.

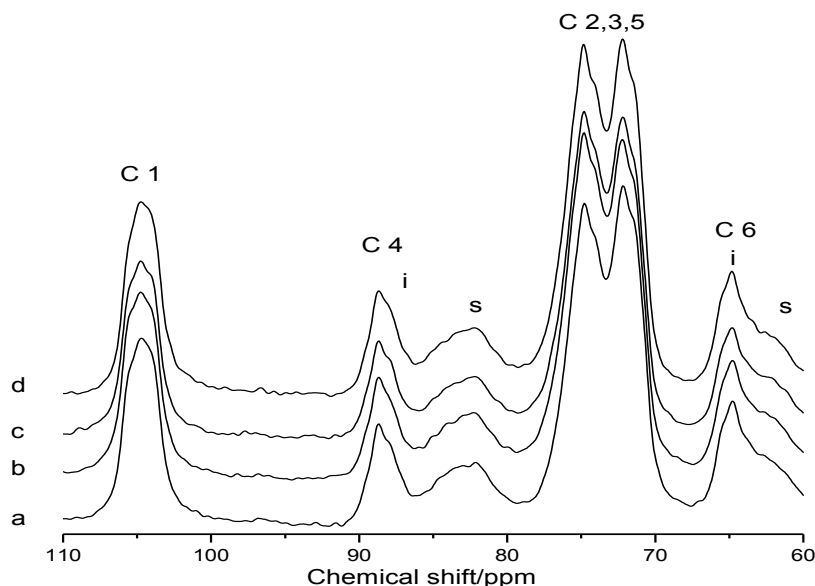


Fig. 6. CP/MAS ^{13}C NMR spectra of the all the pulp samples: (a) without deinking; (b) alkaline deinking; (c) neutral deinking; and (d) enzymatic deinking. Carbon numbers refer to glucose residue of cellulose, labeled i and s and assigned to the interiors and surfaces of crystalline domains.

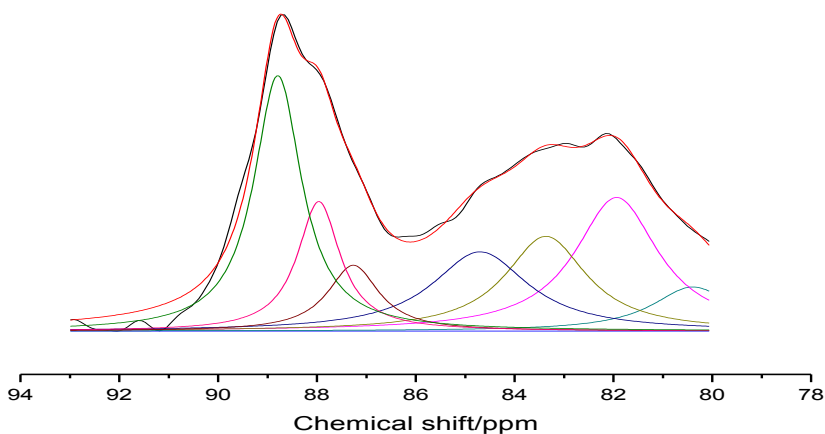


Fig. 7. Lorentzian and Gaussian line shape-fitting of the C-4 spectral region of native fibers

Based on previous research, the C4-region ($\delta 80$ to 92) was resolved by using Gaussian mixed with Lorentzian profiles (Larsson *et al.* 1997). The model used for the fitting procedure includes the use of Lorentzian lines for the three signals from the crystalline cellulose I allomorphs, cellulose I_{α} ($\delta 89.5$), $I(\alpha + \beta)$ ($\delta 88.7$), and I_{β} ($\delta 87.9$), and Gaussian lines for the remaining four signals attributed to non-crystalline cellulose forms, para-crystalline cellulose ($\delta 88.4$), accessible fibril surfaces ($\delta 84.1$ and $\delta 83.2$), and inaccessible fibril surfaces ($\delta 84.9$) (Hult *et al.* 2000; Newman 2004). Figure 7 and Table 4 show the results of the spectral fitting for the cellulose C4-region of the NMR spectra of native pulp.

As can be seen from Table 4, it is apparent that the contents of cellulose I_{α} , I_{β} , $I(\alpha + \beta)$, and para-crystalline cellulose changed differently during the different deinking

processes. The content of the cellulose I_{α} (7.54-8.68%) for all the pulps was relatively constant. After the deinking processes, the contents of the cellulose I ($\alpha + \beta$) and para-crystalline cellulose decreased, while the content of cellulose I_{β} increased. This result may be explained by the fact that during deinking processes the cellulose I ($\alpha + \beta$) and para-crystalline cellulose were converted into the cellulose I_{β} , not the cellulose I_{α} , which was more stable. However, the change tendency was not regular. This may result from the effects of various parameters in different deinking processes that influence the transformation between different cellulose polymorphs and para-crystalline cellulose, including temperature, time, chemicals, *etc.* (Debzi *et al.* 1991). Despite the change of the content of different cellulose polymorphs and para-crystalline cellulose, the total content of crystalline cellulose for all the pulps showed a similar tendency with the change of cellulose crystallinity, which again illustrated that the cellulose crystalline regions were partly destroyed during the deinking processes.

The amount of accessible fibril surfaces decreased from 13.26% to 9.9%, which affected the fibril aggregate size. The average fibril and fibril aggregate sizes are given in Table 4. As can be seen, the trend for the lateral fibril dimensions was in agreement with XRD estimates of the average width of crystallite in 002 (lateral fibril dimension) in Table 3. However, the cellulose fibril size calculated by the NMR method was lower than that obtained by X-ray Diffraction. The probable reason for this difference was that only material within the crystallites appears as crystalline in NMR spectra (Maunu *et al.* 2000). As a consequence, the NMR crystallite size depends on crystalline perfection.

Table 4. Quantification by Spectral Fitting of the Cellulose C4-region of the CP/MAS ^{13}C NMR Spectra

Deinking method	Crystalline cellulose (%)			Para-crystalline cellulose (%)	Accessible fibril surfaces	Inaccessible fibril surfaces (%)	Fibrils size (nm)	Fibrils aggregate size (nm)
	I_{α}	$I(\alpha + \beta)$	I_{β}					
Without deinking	8.04	24.77	9.11	14.65	7.86	13.68	4.8	22.6
Alkaline deinking	7.54	19.93	12.75	11.24	13.26	15.34	3.8	18.5
Neutral deinking	8.68	22.45	11.37	13.29	9.94	13.79	4.5	20.3
Enzymatic deinking	8.41	19.12	12.54	13.55	10.16	13.96	4.3	19.9

The Relationships among the WRV, Hydrogen Bond Models, and Supramolecular Structure of Deinked Fibers

The Water Retention Value (WRV) is a general measure of fiber swelling capacity (Jayme 1958). According to previous research, the hydrogen bond models and cellulose supramolecular structure (crystalline structure) greatly influence the WRV (Kongdee *et al.* 2004; Khantayanuwong *et al.* 2002b; Page and Tydeman 1963; Weise and Paulapuro 1999). For instance, with increasing recycling times, the decrease in the

WRV might have been due to the formation of irreversible hydrogen bonds in the cellulose fibrils of the fibers, or to irreversible aggregation of cellulose microfibrils, or perhaps both factors (Matsuda *et al.* 1994; Wistara and Yong 1999; Hult *et al.* 2001). As always, the main reason accounting for these results is the structure of cellulose. On the one hand, the strength of interfiber bonding is the main contributor to fiber flexibility and swellability (Sheikhi *et al.* 2010). On the other hand, the crystalline regions are interrupted every 60 nm with noncrystalline amorphous regions for all raw materials (Sheikhi *et al.* 2010). The water does not penetrate into crystalline domains of cellulose (Salmen 1988); thus the increase of crystallinity will reduce the water uptake by the cell wall. As a result the swelling ability of fibers will be restricted (Nazhad 1994). The crystalline structure of cellulose and hydrogen bonding substantially affects the swelling capacity of cellulose fibers.

The relationship between the WRV, hydrogen bond models, and crystallinity is shown in Table 5. The water retention values increased significantly after deinking process, in an order of alkaline deinking > enzymatic deinking > neutral deinking, in accordance with the change tendency of the cellulose crystallinity obtained from FTIR and XRD. Meanwhile, the content of the intramolecular hydrogen bonds increased.

Table 5. The Relationship between the WRV, Hydrogen Bond Models, and Crystallinity

Deinking method	WRV (%)	Content of intramolecular hydrogen bonds (%)	Crystallinity Index [CI(XD)]
Without Deinking	143	51.17	68.3
Alkaline deinking	179	62.75	57.9
Neutral deinking	149	55.99	64.2
Enzymatic deinking	166	58.54	61.6

CONCLUSIONS

This work presents an attempt to explain the influence of different deinking processes on the fiber morphology, the content of hydrogen bonds conforming to different models, as well as cellulose supramolecular structure. Along with different deinking processes, pulps differed greatly in structure. After each deinking process, the content of intramolecular hydrogen bonds increased. Meanwhile, the average width of crystallite and fibril aggregate size decreased in accordance with the change of cellulose crystallinity. An alkaline deinking process exhibited the greatest apparent influence on the fiber morphology and structure. The changes observed at the level of the structure of the cellulose fiber may explain the very different effects of different deinking processes on the fibers.

ACKNOWLEDGMENTS

This work was supported by National Natural Science Foundation of China (No.31170551) and (NO. 31200458), Ph.D. Program Foundation of Ministry of Education of China (No.20110172110015), and Foundation for Distinguished Young Talents in Higher Education of Guangdong, China (No.LYM10014) and Fundamental Research Funds for the Central Universities, SCUT (2012ZZ0050).

REFERENCES CITED

- Bajpai, P., and Bajpai, P. K. (1998). "Deinking with enzymes: A review," *Tappi J.* 81(12), 111-117.
- Bennis, H., Benslimane, R., Vicini, S., Mairani, A., and Princi, E. (2010). "Fibre width measurement and quantification of filler size distribution in paper-based materials by SEM and image analysis," *J. Electron Microsc.* 59(2), 91-102.
- Bhuiyan, T. R., and Hirai, N. (2005). "Study of crystalline behavior of heat-treated wood cellulose during treatments in water," *Journal of Wood Science* 51(1), 42-47.
- China Paper Association. (2012). "2011 annual report of China's paper industry," *China Pulp Pap. Ind.* 8, 88-102.
- Chinga, G. (2002). "Structural studies of LWC paper coating layers using SEM and image analysis techniques," Doctorial Thesis of Norwegian University of Science and Technology.
- Claramunt, J., Ardauny, M., and García-Hortal, J.A. (2010). "Effect of drying and rewetting cycles on the structure and physicochemical characteristics of softwood fibers for reinforcement of cementitious composites," *Carbohydrate Polymers* 79(1), 200-205.
- Colom, X., Carrillo, F., Nogues, F., and Garriga, P. (2003). "Structural analysis of photodegraded wood by means of FTIR spectroscopy," *Polymer Degrad. Stab.* 80(3), 543-549.
- Debzi, E. M., Chanzy, H., Sugiyama, J., Tekely, P., and Excoffier, G. (1991). "The Ia \rightarrow I β transformation of highly crystalline cellulose by annealing in various mediums," *Macromolecules* 24(26), 6816-6822.
- Dorris, G., Lapierre, L., Haynes, R. D., and Hill, G. (2003). "Outlook for near-neutral deinking in newsprint production," In: CTP-PTS 6th Advanced Training Course on Deinking.
- Eriksen, Ø., Chinga, G., and Gregersen, Ø. W. (2006). "A mathematical morphology-based method for the quantification of fines in the z-direction of paper," *J. Pulp Paper Sci.* 32(2), 95-99.
- Forsström, J., Andreasson, B., and Wågberg, L. (2005). "Influence of pore structure and water retaining ability of fibers on the strength of papers from unbleached kraft fibers," *Nord. Pulp Pap. Res. J.* 20(2), 176-185.
- Freytag, R., and Donze, J. J. (1983). *Handbook of Fibre Science and Technology*, Vol. I., *Chemical Processing of Fibers and Fabrics, Fundamentals and Application*, Part A, Marcell Dekker, New York.

- Gumusky, E., Usta, M., and Kirci, H. (2003). "The effects of various pulping conditions on crystalline structure of cellulose in cotton linters," *Polym. Degrad. Stab.* 81, 559-564.
- Guo, W. J., Wang, Y., Wan, J. Q., and Ma, Y. W. (2011). "Effects of slushing process on the pore structure and crystallinity in old corrugated container cellulose fibre," *Carbohydr. Polym.* 83, 1-7.
- Heinze, T., and Liebert, T. (2001). "Unconventional methods in cellulose functionalization," *Progress in Polymer Science* 26(9), 1689-1762.
- Hult, E. L., Larsson, P. T., and Iversen, T. (2000). "A comparative CP/MAS C-13-NMR study of cellulose structure in spruce wood and kraft pulp," *Cellulose* 7(1), 35-55.
- Hult, E. L., Larsson, P. T., and Iversen, T. (2001). "Cellulose fibril aggregation – An inherent property of kraft pulps," *Polymer* 42 (8), 3309-3314.
- Hult, E. L., Iversen, T., and Sugiyama, J. (2003). "Characterization of the supermolecular structure of cellulose in wood pulp fibers," *Cellulose* 10(2), 103-110.
- Hult, E. L., Liitiä, T., Maunu, S. L., Hortling, B., and Iversen, T. (2002). "A CP/MAS 13C-NMR study of cellulose structure on the surface of refined kraft pulp fibers," *Carbohydrate Polymers* 49(2), 231-234.
- Ibarra, D., Monte C. M., Blanco, A., Martínez, A. T., and Martínez, M. J. (2012). "Enzymatic deinking of secondary fibers: Cellulases/hemicellulases versus laccase-mediator system," *J. Ind. Microbiol Biotechnol* 39(1), 1-9.
- Jayme, G. (1958). "Properties of wood cellulose II. Determination of and significance of water retention value," *Tappi J.* 41(11), 180-183.
- Jeffries, T. W., Klungness, J. H., Sykes, M. S., and Rutledge-Cropey, K. R. (1994). "Comparison of enzyme-enhanced with conventional deinking of xerographic and laser-printed paper," *Tappi J.* 77(4), 173-179.
- Khantayanuwong, S., Enomae, T., Isogai, A., and Onabe, F. (2002b). "Changes in crystallinity and re-swelling capability of pulp fibers by recycling treatment," *Japan Tappi J.* 56(6), 863-869.
- Kim, S., and Holtzapple, M. T. (2006). "Effect of structural features on enzyme digestibility of corn stover," *Bioresource Technology* 97(4), 583-591.
- Kondo, T., and Sawatari, C. (1996). "A Fourier transform infra-red spectroscopic analysis of the character of hydrogen bonds in amorphous cellulose," *Polymer* 37, 393-399.
- Kongdee, A., Bechtold, T., Burtscher, E., and Scheinecker, M. (2004). "The influence of wet/dry treatment on pore structure-the correlation of pore parameters, water retention and moisture regain values," *Carbohydrate Polymers* 57, 39-44.
- Lapierre, L., Dorris, G., Pitre, D., Bouchard, J., Hill, G., Pembroke, C., and Allen, J. (2002). "Use of sodium sulphite for deinking ONP/OMG at neutral pH. The chemical shows promise in reducing manufacturing costs," *Pulp & Paper Canada* 103(1), 42-45.
- Lapierre, L., Castro, C., Kish, J., Dorris, G., Taylor, C., Allen, J., Hill, G., Merza, J., and Haynes, R. D. (2006). "A 10-day mill trial of near-neutral sulphite deinking. Part III: Overall mill assessment," *Pulp and Paper Canada* 107(5), 39-43.
- Larsson, P. T., Wickholm, K., and Iversen, T. (1997). "A CP/MAS 13 C NMR investigation of molecular ordering in celluloses," *Carbohydr Res* 302, 19-25.
- Liao, Z. D., Huang, Z. Q., Hu, H. Y., Zhang, Y. J., and Tan, Y. F. (2011). "Microscopic structure and properties changes of cassava stillage residue pretreated by mechanical activation," *Bioresource Technology* 102(17), 7953-7958.

- Liu, R., Yu, H., and Huang, Y. (2005). "Structure and morphology of cellulose in wheat straw," *Cellulose* 12(1), 25-34.
- Mansfield, S. D., DeJong, E., Stephens, R. S., and Saddler, J. N. (1997). "Physical characterization of enzymatically modified kraft pulp fibers," *J. Biotechnology* 57, 205-216.
- Maréchal, Y., and Chanzy, H. (2000). "The hydrogen bond network in IB cellulose as observed by infrared spectrometry," *Journal of Molecular Structure* 523(1-3), 183-196.
- Marcovich, N. E., Reboredo, M. M., and Aranguren, M. I. (2001). "Modified wood flour as thermoset fillers. II. Thermal degradation of wood flours and composites," *Thermochimica Acta* 372(1-2), 45-57.
- Matsuda, Y., Isogai, A., and Onabe, F. (1994). "Effects of thermal and hydrothermal treatments on the reswelling capabilities of pulps and papersheets," *J. Pulp Paper Sci.* 20(11), 323-327.
- Maunu, S., Liitia, T., Kauliomaki, S., Hortling, B., and Sundquist, J. (2000). "¹³C CPMAS NMR investigations of cellulose polymorphs in different pulps," *Cellulose* 7(2), 147-159.
- Miyamoto, H., Ago, M., Yamane, C., Seguchi, M., and Ueda, K. (2011). "Supermolecular structure of cellulose/amylose blends prepared from aqueous NaOH solutions and effects of amylose on structural formation of cellulose from its solution," *Carbohydrate Research* 346(6), 807-814.
- Mohkami, M., and Talaiepour, M. (2011). "Investigation of the chemical structure of carboxylated and carboxymethylated fibers from waste paper via XRD and FTIR analysis," *BioResources* 6(2), 1988-2003.
- Nazhad, M. M. (1994). "Fundamentals of strength loss in recycled paper," Doctoral dissertation, The University of British Columbia.
- Newman, R. H. (2004). "Carbon-13 NMR evidence for cocrystallization of cellulose as a mechanism for hornification of bleached kraft pulp," *Cellulose* 11(1), 45-52.
- Oh, S. Y., Yoo, D. Il., Shin, Y., Kim, C. H., Kim, H. Y., Chung, Y. S., Park, W. H., and Youk, J. H. (2005). "Crystallines structure analysis of cellulose treated with sodium Hydroxide and carbon dioxide by means of X-ray diffraction and FTIR spectroscopy," *Carbohydrate Research* 340(15), 2376-2391.
- Page, D. H., and Tydeman, P. A. (1963). "Transverse swelling and shrinkage of softwood tracheids," *Nature* 199(4892), 471-472.
- Pan, X. J. (2008). "Role of functional groups in lignin inhibition of enzymatic hydrolysis of cellulose to glucose," *Journal of Biobased Materials and Bioenergy* 2, 25-32.
- Popescu, C. M., Singurel, G., Popescu, M. C., Vasile, C., Argyropoulos, D., and Willför, S. (2009). "Vibrational spectroscopy and X-ray diffraction methods to establish the differences between hardwood and softwood," *Carbohydrate Polymers* 77(4), 851-857.
- Rebuzzi, F., and Evtuguin, D.V. (2006). "Effect of glucuronoxylan on the hornification of Eucalyptus globulus bleached pulps," *Macromol. Symp.* 232, 121-128.
- Salmen, L. (1988). "Crystallinity effects on mechanical properties of H-bond-dominated solids: Comments on the recent article by Batten and Nissan," *Tappi J.* 70(12), 190-193.

- Schwanninger, M., Rodrigues, J. C., Pereira, H., and Hinterstoisser, B. (2004). "Effects of short-time vibratory ball milling on the shape of FT-IR spectra of wood and cellulose," *Vibrational Spectroscopy* 36(1), 23-40.
- Sheikhi, P., Talaeipour, M., Hemasi, A. M., Eslam, H. K., and Gumuskaya, E. (2010). "Effect of drying and chemical treatment on bagasse soda pulp properties during recycling," *BioResources* 5(3), 1702-1716.
- Shrinath, A., Szewczak, J. T., and Bowen, I. J. (1991). "A review of ink-removal techniques in current deinking technology," *Tappi J.* 74(7), 85-93.
- Wan, J. Q., and Ma, Y. W. (2004). *Waste Papermaking and Pollution Control*, China Light Industry Press, Beijing.
- Wan, J. Q., Wang, Y., and Xiao, Q. (2010). "Effects of hemicellulose removal on cellulose fiber structure and recycling characteristics of eucalyptus pulp," *Bioresource Technology* 101(12), 4577-4583.
- Wei, G. B. (2009). "Studies on the properties of secondary fiber in different deinking methods," South China university of Technology, Guangzhou, China.
- Wei, H. L., Shi, S. L., and Pei, J. C. (2007). "SEM analysis of eucalyptus fiber surface treated by laccase," *Transactions of China Pulp and Paper* 22(4), 65-67.
- Weise, U., and Paulapuro, H. (1999). "Effect of drying and rewetting cycles on fibre swelling," *Journal of Pulp and Paper Science* 25(5), 163-166.
- Wistara, N., and Yong, R. A. (1999). "Properties and treatments of pulps from recycled paper. Part I: Physical and chemical properties of pulps," *Cellulose* 6(4), 291-324.

Article submitted: October 17, 2012; Peer review completed: January 17, 2013; Revised version received and accepted: March 18, 2013; Published: March 26, 2013.